Applied Materials Today 17 (2019) 104–111

Contents lists available at ScienceDirect

Applied Materials Today

journal homepage: www.elsevier.com/locate/apmt

Sulfur treated 1D anodic TiO_2 nanotube layers for significant photo- and electroactivity enhancement

Milos Krbal[a,*], Siowwoon Ng[b], Martin Motola[a], Ludek Hromadko[a], Filip Dvorak[a], Vit Prokop[a], Hanna Sopha[a,b], Jan M. Macak[a,b,*]

[a] Center of Materials and Nanotechnologies, Faculty of Chemical Technology, University of Pardubice, Nam. Cs. Legii 565, 53002 Pardubice, Czech Republic
[b] Central European Institute of Technology, Brno University of Technology, Purkyňova 123, 612 00 Brno, Czech Republic

ARTICLE INFO

Article history:
Received 28 March 2019
Received in revised form 5 July 2019
Accepted 28 July 2019

Keywords:
TiO_2 nanotube layers
Sulfurization
Photocurrent
Photocatalysis
Photoelectrochemistry

ABSTRACT

In this work, we show that sulfur treated 1D anodic TiO_2 nanotube layers lead to improved photoelectrochemical and catalytic properties compared to the blank nanotube layers. This treatment was performed in the evacuated quartz ampoules in the temperature range from 250 to 450 °C. Inspection of the sulfurized nanotube layers via scanning electron microscopy (SEM) and X-ray diffraction (XRD) has disclosed a gradual crystal growth within nanotube walls, represented by TiS_2 or TiS_3 phases. Optimally sulfurized TiO_2 nanotube layers exhibit 3 times enhanced photocurrent in the UV spectral region, compared to the blank counterpart, with a shift of the light absorption up to the wavelength of 550 nm. In addition, the photocatalytic decomposition of a methylene blue aqueous solution using a wavelength of 365 nm is gradually improved with increasing sulfurization temperature. The highest photocatalytic decomposition rate is 2.3 times larger compared to the blank TiO_2 nanotube layer. The application of sulfurized TiO_2 nanotube layers for the electrocatalytic hydrogen evolution is also discussed.

1. Introduction

Among metal oxide semiconductors, titanium dioxide (TiO_2) has shown to be the one of the most efficient, non-toxic, chemically and photochemically stable material (under long-term exposure to irradiation) for electrochemical applications such as a hydrogen evolution [1,2], photocatalysis [3–5], and dye sensitized and hybrid solar cells [6,7]. In order to enhance the photoactivity, TiO_2 has been produced in many forms, namely, nanoparticles, nanowires, nanorods or self-organized nanotube layers with consequence on the total surface area and photogeneration of electron-hole pairs with a sufficiently high concentration [8–10]. Especially, the latter mentioned one-dimensional (1D), ordered nanostructures offer the advantage of directed charge transport as well as a long lifetime of photogenerated charge carriers.

The major limitation of the outstanding performance of pure TiO_2 is its absorption in the UV light spectral region (the band gap of TiO_2 in the anatase phase is 3.2 eV) and thus only a small portion of the solar spectrum can be efficiently harvested. To overcome this drawback, additional engineering of TiO_2 via doping with metals [11–14] or non-metals [15–20], anodic reduction [21,22], creation of black TiO_2 [23,24], using of plasmonic Ag nanoparticles [13,25] and coating of TiO_2 by secondary materials with lower bandgap [26] was used to shift the light absorption into the visible spectral region.

Recently, non-metal doping has been found as one of the consistent ways how to desirably tune the band gap of TiO_2. In contrast to metal doping, that typically induces extra recombination centres as well as low thermal stability [20], the incorporation of N, C, chalcogenides or halides circumvents the aforementioned shortcomings and thus essentially improves the solar light conversion efficiency. For instance, sulfur doped (S-doped) TiO_2 nanoparticles have shown substantially enhanced photocatalytic performance, when operated in the visible (VIS) spectral region [27–31]. Based on Density Functional Theory (DFT) calculations, the VIS spectral region photoactivity of S-doped TiO_2 exclusively originates from the substitution of Ti or O atoms by S atoms, whereas incorporation of S atoms into the interstitial position has been proven to be energetically unfavourable [31]. In addition, in the case of Ti-rich TiO_2, S atoms should predominantly enter into the anion sub-lattice, creating new energy levels within the bandgap. However, experimental findings by XPS have disclosed that S atoms in TiO_2 mainly prefer the cation substitution S^{4+}/S^{6+} in the form of SO_3^{2-}/SO_4^{2-},

* Corresponding authors.
E-mail addresses: milos.krbal@upce.cz (M. Krbal), jan.macak@upce.cz (J.M. Macak).

https://doi.org/10.1016/j.apmt.2019.07.018

rather than the anion counterpart S^{2-}, probably due to the larger anionic radius of S^{2-} in comparison to that of O^{2-} [32]. Also, the cation substitution generates the red shift of the absorption edge and thus enhances the VIS spectral region photoactivity. It has been reported that the presence of both cationic and anionic S species strongly depends on the preparation conditions. For example, S-doped TiO_2 nanoparticles prepared by means of annealing of TiS_2 nanoparticles in air showed residual S^{2-} units [33], whereas S^{4+}/S^{6+} are the characteristic features after the sol-gel synthesis from titanium (IV) isopropoxide and thiourea [33] or H_2SO_4 [32] precursors or via sulfidation of P25 TiO_2 nanoparticles in gaseous H_2S [34].

To our knowledge, the research of S-doped TiO_2 in terms of increased photoactivity has been mainly performed on nanoparticles, while only a brief report on sulfurized TiO_2 nanotube layers via H_2S at 380 °C or 500 °C has been shown [29,35,36]. Recently, TiO_2 nanotube layers sulfurized at 450 °C for 3 h were successfully employed as electrode of lithium–ion microbatteries [37,38]. However, a systematic study on sulfur treated 1D ordered TiO_2 nanostructures, such as self-organized TiO_2 nanotube layers, has not been conducted yet. To close this gap, we optimized sulfurization conditions in the temperature range from 250 to 450 °C at different durations to achieve the maximum photocurrent collection, yet protecting the structural integrity of the nanotubes. We also present potential applications of the sulfurized TiO_2 nanotube layers for the photocatalytic decomposition of the methylene blue aqueous solution and for the electrocatalytic hydrogen evolution.

2. Experimental

Prior to anodization, the Ti foils (Sigma-Aldrich, 0.127 mm, 99.7% purity) were degreased by sonication in isopropanol and acetone, then rinsed with isopropanol and dried in air. The electrochemical setup consisted of a two-electrode configuration using a platinum foil as the counter electrode, while the Ti substrates (working electrodes) were pressed against an O-ring of the electrochemical cell, leaving 1 cm^2 opening exposed to the electrolyte. Ti foils of a size of 0.75×3 cm^2 were used as working electrodes for the production of TiO_2 nanotube layers on stripes. Electrochemical experiments were carried out at room temperature employing a high-voltage potentiostat (PGU-200 V, IPS Elektroniklabor GmbH).

The TiO_2 nanotube layers, with a thickness of ~20 μm and a nanotube diameter of ~110 nm, were prepared by anodization of Ti foils at 60 V (with sweep rate of 1 V/s) for 4 h in an ethylene glycol based electrolyte containing 170 mM NH_4F and 1.5 vol.% of deionized H_2O. After the anodization, the grown TiO_2 nanotube layers were rinsed and sonicated in isopropanol and dried in air. The as-prepared amorphous nanotube layers were further crystallized to the anatase phase by annealing at 400 °C for 1 h in air atmosphere with a heating rate of 2 °C/min and natural cooling carried out in a muffle oven.

The sulfurization of TiO_2 nanotube layers was performed as follows: TiO_2 nanotube layers along with 0.2 g of pure sulfur were placed into cleaned quartz ampoules which were subsequently evacuated to 10^{-3} Pa and sealed. In the next step, the evacuated ampoules were exposed to temperatures in the range from 250 °C to 400 °C (50 °C step) all for 7 min, and 450 °C for 7, 30 min and 3 h with a heating rate of 5 °C/min and then naturally cooled to the room temperature inside the furnace.

The structure and morphology of the TiO_2 nanotube layers were characterized by an X-ray diffractometer (Empyrean, Malvern Panalytical) and field-emission scanning electron microscope (FE-SEM JEOL JSM 7500 F).

All photocurrent measurements were carried out in an aqueous electrolyte containing 0.1 M Na_2SO_4 at a constant potential of 0.4 V vs 3 M Ag/AgCl, employing a photoelectric spectrophotometer (Instytut Fotonowy) connected with the modular electrochemical system AUTOLAB (model "PGSTAT 204", Metrohm Autolab B.V.) operated with *Nova 1.10* software. A three-electrode cell with a flat quartz window was employed with a Ag/AgCl reference electrode, a Pt wire counter electrode and the anodized and annealed Ti substrate as working electrode, pressed against an O-ring of the electrochemical cell leading to an irradiated sample area of 0.28 cm^2. The wavelength dependence of photocurrent densities was measured using a monochromatic light source provided by a 150 W Xe lamp and a universal grating monochromator, with a bandwidth of 5 nm. The monochromatic light source employed for excitation was controlled using a shutter between light and dark phases with an interval of 10 s. Further to that, the photocurrent density transients were measured at constant wavelengths of 360 nm and 450 nm (these wavelengths were selected based on the maximum photocurrent density, representing the highest photoresponse in the UV and VIS light spectrum, respectively). Cyclic voltammograms were recorded in the potential range from −0.4 V to 1 V vs. 3 M Ag/AgCl with a sweep rate of 5 mV/s, starting at 0 V towards positive voltages in the dark.

The photocatalytic decomposition of an aqueous methylene blue (MB) solution with an initial concentration of 1×10^{-5} M was performed in a quartz cuvette with irradiation by a LED-based UV lamp with a power output 10 W and a wavelength of 365 ± 5 nm. Prior to the MB photodecomposition, probed samples with an area of 0.75×3 cm^2 were immersed in a quartz cuvette containing 3.5 ml MB for 1 h with constant stirring to achieve a dye adsorption–desorption equilibrium. The absorbance of the MB solution was periodically measured (10 or 30 min interval) by a UV–VIS spectrometer (S-200, Boeco) at a wavelength of 670 nm to monitor the decomposition rates.

3. Results and discussion

The optimization process was carried out within two complementary steps. First, the time of sulfur treatment was reduced from 3 h to 7 min at a constant temperature of 450 °C. In the second step, the sulfur treatment duration was fixed at 7 min while the temperature was gradually decreased from 450 °C to 250 °C with 50 °C step. Fig. 1A shows that the incident photon-to-electron conversion efficiency (IPCE) across the spectral range from 310 to 550 nm significantly increases with decreasing the sulfurization time from 3 h to 7 min at a constant temperature of 450 °C. Further, decreasing the temperature from 450 °C to 400 °C results in two changes, namely: ĩ5% drop in IPCE in the wavelength range from 300 to 340 nm and ĩ2 nm red-shift in the wavelength range from 350 to 370 nm. However, the IPCE does not change with a subsequent decrease of the temperature to 350 °C. One can see from Fig. 1B that sulfurization at temperatures lower than 350 °C leads to a reduction in photoresponse in both UV and VIS spectral regions, which indicates that the sulfurization at 350 and/or 400 °C for 7 min represents the optimal experimental conditions to obtain the most effective photocurrent generation via sulfur treated TiO_2 nanotube layer.

In contrast to the blank TiO_2 nanotube layer, sulfurized TiO_2 nanotube layers show superior photoresponse, as shown in Fig. 1. More specifically, the IPCE values were about 3 times higher for optimally sulfurized TiO_2 nanotube layers (350 °C and 400 °C, 7 min) in the UV spectral region, reaching 60% IPCE at 360 nm shown in Fig. 1A, as compared with the blank counterpart. This phenomenon can be ascribed to the annihilation of surface defects in TiO_2 [26,31], resulting in significant inhibition of the charge carrier recombination.

Similar results have been very recently reported on S-TiO_2 nanoparticles prepared from DMSO [39] as well as on TiO_2 nanotube layers sulfurized by a mixture of H_2/H_2S at 500 °C for 30 min

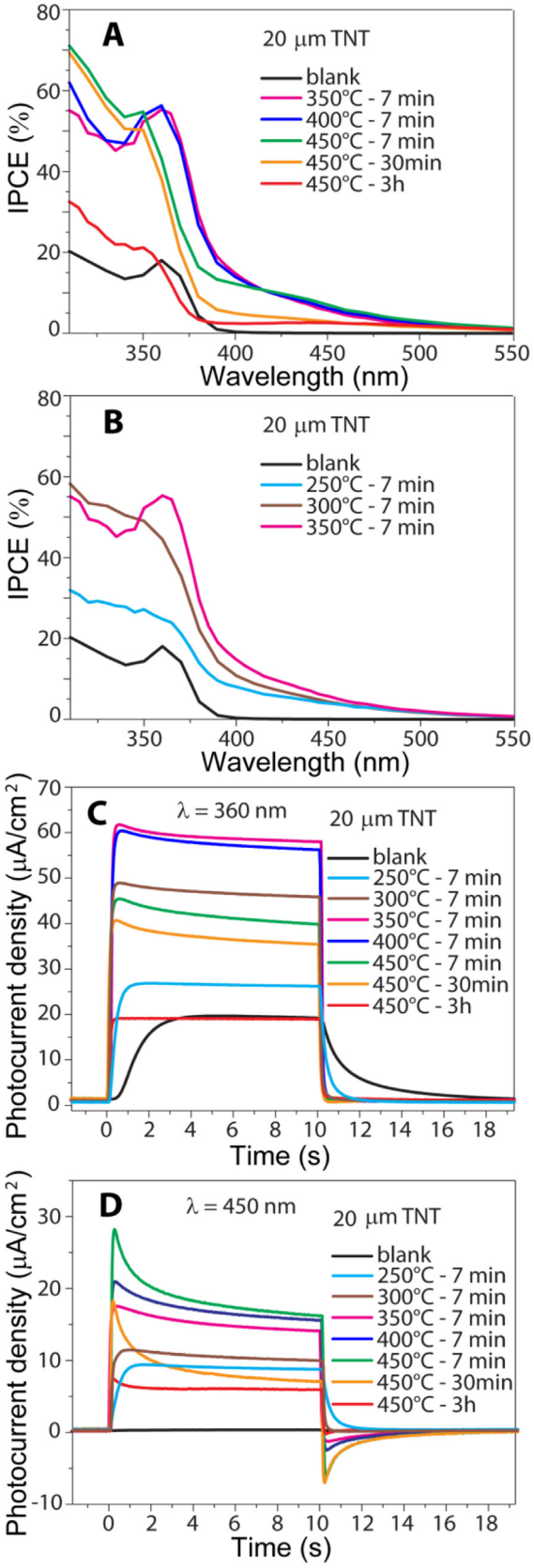

Fig. 1. A) and B) Incident photon-to-electron conversion efficiency (IPCE) of sulfurized TiO_2 nanotube layers in the temperature ranges from 350 to 450 °C and from 250 to 350 °C, respectively. C) and D) photocurrent transients at 360 nm and 450 nm, respectively, recorded for blank and sulfurized TiO_2 nanotube layers at different conditions.

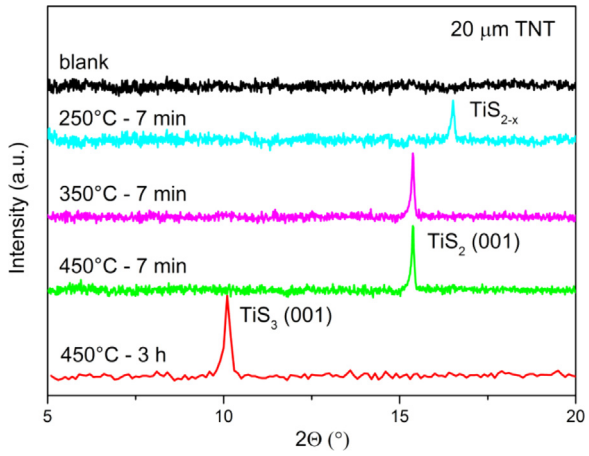

Fig. 2. XRD patterns of the blank and sulfurized TiO_2 nanotube layers at 250 °C, 350 °C, 450 °C for 7 min and 450 °C for 3 h. The 2Θ area selection demonstrates the formation of characteristic peaks of different Ti-S phases.

[35]. It is fair to stress that a pure H_2S treatment under the same conditions demonstrates lower IPCE in contrast to H_2/H_2S [29,35]. However, the latter approaches exhibited significantly lower photoresponse in the visible spectral region in comparison with sulfurized TiO_2 nanotube layers under optimum conditions presented in this work.

As a consequence, upon irradiation, the photocurrent response of sulfur treated TiO_2 nanotube layers rises abruptly in comparison with the sluggish charge transfer kinetics observed in the blank nanotube layer in Fig. 1(C). The incorporation of S atoms into the TiO_2 nanotube layers broadens the photocurrent generation from the UV spectral region to 550 nm, which is in a good agreement with previous studies on S-doped TiO_2 nanoparticles [31]. The extension to the VIS light absorption has been described via DFT as substitutional anionic doping of S within TiO_2 host matrix, forming S3p orbitals at the top of the valance band maximum and mixing them with O2p orbitals [30], which reduce the band gap.

The highest photoresponse in the VIS spectral region was observed for nanotube layers sulfurized for 7 min in the temperature range of 350–450 °C, as shown in Fig. 1A and D. In the case of temperatures lower than 350 °C, the sulfurization process seems to be insufficient, whereas sulfurization at 450 °C induces additional charge traps. Both aspects will be discussed based on the crystallography and the surface morphology of sulfurized TiO_2 nanotube layers. Complementary diffuse reflectance spectra were also recorded for the blank and sulfurized TiO_2 nanotube layers and are shown in Figure S1. These spectra are in good agreement with the IPCE values.

To unravel the role of the S-based structure on the photocurrent enhancement, we collected the X-ray diffraction patterns of the blank and sulfurized TiO_2 nanotube layers. At this point, we only singled out TiO_2 nanotube layers for which trends in the IPCE curves showed substantial changes in intensity and the red-shift responses, namely: sulfurized at 250 °C, 350 °C (optimized condition), 450 °C for 7 min and 450 °C for 3 h and blank (as the reference sample), respectively. Fig. 2 displays XRD patterns recorded in the range of 2Θ from 5 to 20°, where the dominant characteristic peaks of Ti-S phases can be found. One can see that the blank TiO_2 nanotube layer does not feature any peak in the studied range of 2Θ. Upon sulfurization of TiO_2 nanotube layers at 250 °C for 7 min, a diffraction peak appears at 2Θ ~ 16.5° which corresponds to the TiS_{2-x} or Ti-S-O phase with unidentified composition. When the sulfurization was increased to 350 °C, a new diffraction peak emerges at 2Θ ~ 15.4° which can be assigned to the TiS_2 phase, adopting the hexagonal structure with space group P $\bar{3}$ m1 [40], while the

former TiS_{2-x} phase disappears. Since the sulfurization process is performed under the atmosphere with significant surplus of sulfur, the sulfur treatment at 450 °C leads to the recrystallization of TiS_2 into a new phase TiS_3, with its characteristic diffraction peak at 2Θ ~ 10.3°, possessing the monoclinic structure with space group $P2_1/m$ [41]. Based on the XRD evaluation and in comparison with the IPCE results, one comes to a conclusion that mild sulfurization (350 and 400 °C for 7 min), creating TiS_2 phase within nanotube walls, is the most efficient in terms of the photocurrent generation among all conditions used in this study.

Nevertheless, the Bragg diffraction analysis is not the surface sensitive method. To illustrate the surface composition we performed XPS analysis of sulfurized sample at 250, 350 °C for 7 min (optimum conditions for photocurrent harvesting), 450 °C for 30 min (the optimum condition for the photocatalytic decomposition of the MB aqueous solution) and 450 °C for 3 h (final state) to elucidate the oxidation states of the sulphur upon different sulfurization conditions.

One can see from Fig. 3 that upon analysis of the S2p XPS spectra, it was identified a few different sulphur specimens, namely S^{2-} with the binding energy, $E_B(2p_{3/2}) = 160.2$ eV [38,42], S_2^{2-} with the binding energy, $E_B(2p_{3/2}) = 161.5$ eV [38,42], $(S_x)^{2-}$ with $E_B(2p_{3/2}) = 162–163.8$ eV assigned to polysulphides with a variable number of sulphur atoms in the chain [43], elemental S with $E_B(2p_{3/2}) = 163.8$ eV [43], $(SO_3)^{2-}$ unit with $E_B(2p_{3/2}) = 166.4$ eV 166.5 and $(SO_4)^{2-}$ unit with $E_B(2p_{3/2}) = 168.6$ eV [32]. It is apparent that $(S_x)^{2-}$ polysulphides gradually transform into S_2^{2-} and S^{2-} structural units with increasing temperature at which sulfurization proceeds.

Upon sulfurization at 450 °C for 3 h exclusively S_2^{2-} and S^{2-} ions can be considered as a dominant oxidation states of sulphur species on the surface of the TiO_2 nanotube layers. The results manifest that the surface composition is complex rather than uniform demonstrated by XRD. There are at least two aspects which can describe the distinct structural information obtained from XRD and XPS. First, XPS probes only the surface area while XRD the whole volume of all samples. Second, in this work double wall TiO_2 nanotube layers [44,45] were used. The outer shell on nanotubes is formed from a "pure" TiO_2 while the inner shell is porous containing some dopants (C, F,..) and thus the inner shell is more defective. It seems, from Fig. S2, that the TiO_2 in the inner shell reacts readily with the vapour sulphur in comparison with TiO_2 in the outer shell.

Further, the morphology of the blank and sulfurized TiO_2 nanotube layers was characterized by SEM. Fig. 4 left column shows top-view SEM images of a blank TiO_2 nanotube layer annealed at 400 °C and sulfurized TiO_2 nanotube layers at 350 °C, 400 °C, 450 °C for 7 min, 450 °C for 30 min and 450 °C for 3 h. The corresponding representative cross-sectional SEM images, taken at the bottom part of the nanotube layers, are shown in the right column of Fig. 4. An obvious increase of the wall thicknesses with the increasing sulfurization temperature and time unequivocally confirms the reaction of TiO_2 with elemental sulfur in the vapour phase and the growth of new Ti-S or Ti-O-S phases depending on the sulfurization conditions. In order to demonstrate that the TiO_2 nanotube layers were homogeneously treated with sulfur throughout the whole thickness of all layers (approx. 20 μm), cross-sectional SEM analyses of the sulfurized TiO_2 nanotube layers were carried out.

These analyses verified that the nanotubes were indeed properly sulfurized from the top to the bottom part as well as within the interiors and exteriors for all nanotube layers. The surface of the blank TiO_2 nanotubes is covered by typical ripples on the tube walls connecting the nanotubes together without any other obvious features in between these ripples. Upon sulfurization at 350 °C, the number of these ripples was dramatically reduced and the tube wall surface was overlaid with flat crystals well adhered to the orig-

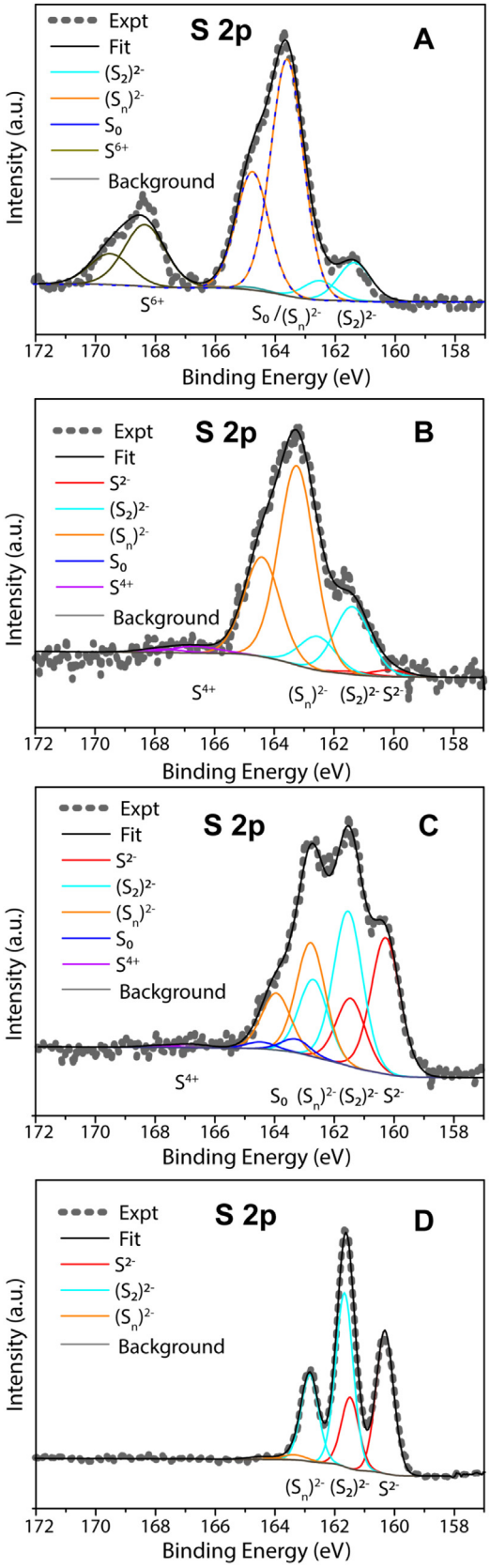

Fig. 3. XPS spectra of the blank and sulfurized TiO_2 nanotube layers at 250 °C, 350 °C, 450 °C for 30 min and 450 °C for 3 h. The 2Θ area selection demonstrates the formation of characteristic peaks of different Ti-S phases.

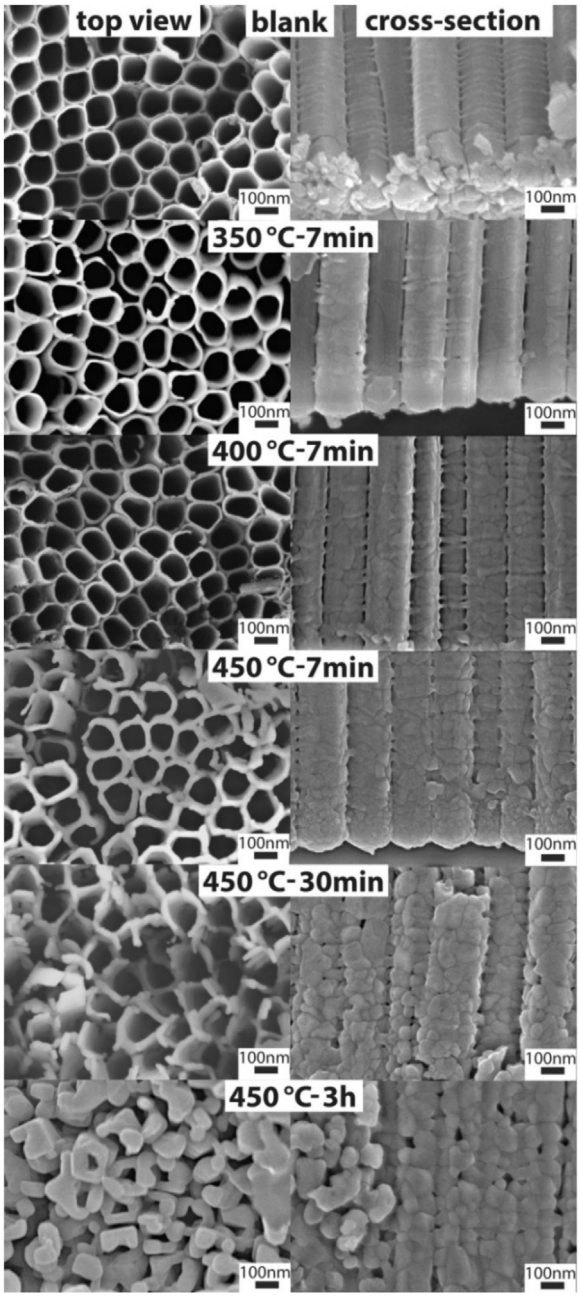

Fig. 4. (Left column) top-view and (Right column) cross-section SEM images of a blank self-organized TiO_2 nanotube layer and sulfurized TiO_2 nanotube layers at 350 °C, 400 °C, 450 °C for 7 min, 450 °C for 30 min and 450 °C for 3 h.

inal TiO_2 nanotubes. With increasing sulfurization temperature, the newly formed crystals gradually became more pronounced. For the temperature of 450 °C (and with increasing durations), the growing crystals gradually interrupt the original continuous nanotube bodies and form rather large connected crystals. We assume that this phenomenon can be responsible for the dramatic decrease in IPCE, observed in Fig. 1, rather than the change in crystal phase from TiS_2 to TiS_3, as discussed along the observations in Fig. 2.

In general, transition metal dichalcogenides (TMDCs), such as TiS_2 presented here, have been successfully employed in many applications [46–48]. Among them, the photocatalytic decomposition of organic dyes represents a prototypical model application of removing pollutants from various wastewaters [31]. In this work, we have performed the photocatalytic decomposition of a methylene blue aqueous solution (MB) under UV light irradiation at the

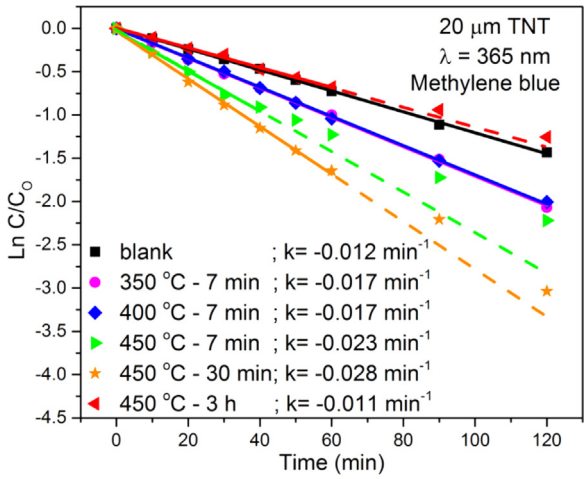

Fig. 5. Photocatalytic decomposition of an aqueous MB solution using blank TiO_2 nanotube layers and layers sulfurized at 350, 400, 450 °C for 7 min and 450 °C for 30 min and 3 h. Solid lines represent the linear fit of the experimental data and dashed lines are extended fits for the experimental data which are not included in the fit.

wavelength of 365 nm. The results in Fig. 5 manifest that the photocatalytic decomposition of MB accelerates with an increasing degree of sulfurization. In this experimental set, the best conditions of sulfurization were found to be 450 °C for 30 min, having the photodecomposition rate constant 0.028 min^{-1} which is about 2.3 times higher, compared to the rate constant of the blank TiO_2 nanotube layer (0.012 min^{-1}).

While the observed trend is not fully in an agreement with the photocurrent results, the explanation of the phenomenon can be described as follow. When the photocurrent is collected, the photogenerated electrons have to be transported to the positive electrode across the whole thickness of nanotube layer. As aforementioned, sulfurization of TiO_2 nanotube layers at 450 °C produces more 3D crystals rather than flat crystals formed at lower temperatures and thereby generates more electron traps. Also, an increased number of the S-Ti-S triplet layers connected with Van der Waals bonds within the hexagonal phase could significantly suppress the electron transfer in the direction perpendicular to the basal plane [48]. Both aspects have a detrimental effect on the charge carrier transport.

Contrary, the photocatalysis proceeds on the solid/liquid interfaces. The low temperature sulfur treatment helps to annihilate surface states by TiS_2 flat crystals, which are well connected to the TiO_2 nanotube walls. This might explain the enhancement of photocatalytic decomposition of the MB, when sulfurized at 350 and 400 °C, in contrast to the blank counterpart, while their photodecomposition rate constants (k = −0.017 min^{-1}) are similar. It is obvious from SEM images that sulfurization at 450 °C with increasing time augments the surface roughness of the TiO_2 nanotube walls by means of nanotube recrystallization which enlarges the effective surface area. It was described in the literature that in the case of TMDCs, the catalytic active centres are located on the edge sites of individual triplet layer [48]. We believe that the distinct Ti-S crystallites might increase the number of active centres, which accelerates the photocatalytic decomposition of the MB solution with increasing degree of sulfurization.

On the other hand, the SEM top view image of the sulfurized TiO_2 nanotube layer at 450 °C for 3 h shows a noticeable increase of the nanotube wall thickness resulting in the reduction of tube diameters as well as in a decrease of gaps between nanotubes. These morphological changes markedly reduced the active surface area resulting in a lower photocatalytic activity of the heavily sulfurized nanotube layer. Last but not least, Figure S3 shows the stability

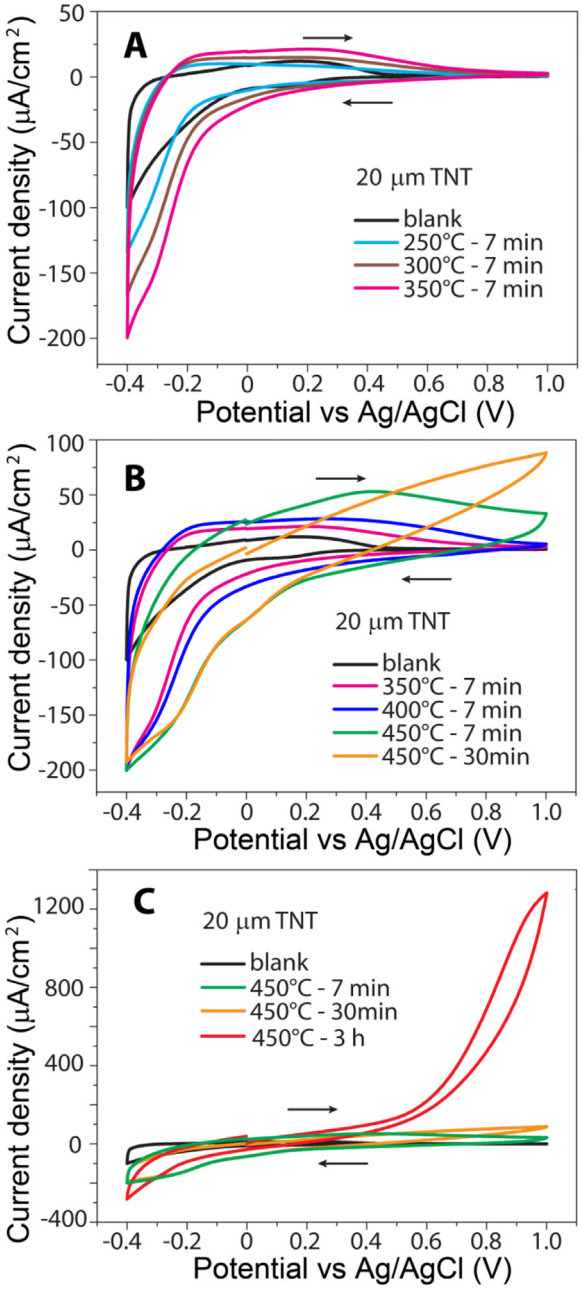

Fig. 6. CV curves showing dark current densities recorded for TiO_2 nanotube layers sulfurized at temperatures A) from 250 to 350 °C for 7 min, B) from 350 to 450 °C for 7 min and 450 °C for 30 min and 450 °C for 7 and 30 min, and 3 h. The dark current density of a blank TiO_2 nanotube layer is included in all figures as the reference.

of the photocatalytic performance of the sulfurized TiO_2 nanotube at 400 °C for 7 min recorded for 2 different tests with one sample carried out with a 5 day span.

Next to the utilization as photocatalysts, the family of TMDCs has also attracted significant attention in the electrocatalytic hydrogen evolution due to their high intrinsic activity in this reaction [35,48–53]. To exploit sulfurized TiO_2 nanotube layers for the electrocatalytic hydrogen evolution, we recorded numerous CV curves in the range of potentials from −0.4 to 1 V vs Ag/AgCl under the dark condition. Results are summarized in Fig. 6 for various sulfur treatments. One can see from Fig. 5A that the current densities at −0.4 V vs Ag/AgCl gradually increase with the increasing sulfurization temperature from 250 to 350 °C. The highest value of −200 μA/cm^2 is obtained for the TiO_2 nanotube layer sulfurized at 350 °C, while the blank counterpart generates only −100 μA/cm^2.

Although sulfurization at temperatures higher than 350 °C does not enhance the current density at −0.4 V, the cathodic peak is extended to the more positive potentials, as shown in Fig. 6B. It is noteworthy that the obtained results are comparable with recently published reports on TiS_2 nanosheets [51] and about an order of magnitude lower with respect to the hydrogen evolution reaction processed using TiS_2 QDs [51] and rather worse than a combination of TiS_2 – Pt [54].

The Tafel slopes demonstrate the benefit of the sulfurization of TiO_2 nanotube layers for H_2 evolution (Fig. S4). Compared with blank TiO_2 nanotube layers, a gradual decrease of Tafel values can be observed for sample after sulfurization until 350/400 °C for 7 min, namely from 125 mV/dec to 97 mV/dec. Sulfurization at 450 °C leads to increase the Tafel values again. While the present results are comparable with TiS_2 nanosheets [51,54] but worse in comparison with standard Pt/C 30 mV/dec [54,55] or other recently reported advanced materials [51,54,56] they demonstrate a useful strategy for further optimalization of low cost electrocatalytic hydrogen evolution catalysts.

On top of that, TiO_2 nanotube layers sulfurized at 450 °C exhibit also the anodic oxidation peak in the potential range of −0.4 to 1 V. The intensity of this peak dramatically increases with the sulfurization time (see Fig. 6C). For example, TiO_2 nanotube layers exposed to the sulfur atmosphere for 3 h acquire a significant current density of 1.2 mA/cm^2 at 1 V which is in strong contrast with a few μA/cm^2 monitored on the blank and other sulfurized TiO_2 nanotube layers treated at milder conditions than 450 °C for 3 h. In combination with XRD analyses, we believe that the observed anodic peak is directly linked to the presence of the TiS_3 phase formed on the TiO_2 nanotube layers, whereas the TiS_2 phase does not succumb to the obvious oxidation process until 1 V vs Ag/AgCl.

4. Conclusions

In conclusion, we presented a systematic study on sulfur treated 1D anodic TiO_2 nanotube layers produced in the evacuated quartz ampoules in the range of temperatures from 250 to 450 °C with different durations from 7 min to 3 h. We showed that the highest IPCE and at the same time the maximum red shift in the light absorption was observed for the optimal sulfurization conditions: 350 °C for 7 min. Corresponding XRD patterns revealed that the TiO_2 nanotubes consist of the TiS_2 phase. In contrast, long-term sulfurization at 450 °C (herein shown for 3 h) leads to the formation of the TiS_3 phase within the TiO_2 nanotubes, confirmed by XRD. Next, we demonstrated that the sulfurization modifies the morphology and surface area of TiO_2 nanotubes by further recrystallization. Although the crystal formation on the surface of TiO_2 nanotubes becomes stronger with increasing temperature, nanotube layers maintain their structural integrity and do not collapse in any case. Further, we presented that the photocatalytic decomposition of MB using a wavelength of 365 nm was gradually enhanced with increasing sulfurization temperature until 450 °C for 30 min compared to the blank nanotube layers. Nanotube layers sulfurized at 450 °C for 3 h operated at similar rates as the blank layers. Finally, we demonstrated the potential application of sulfurized TiO_2 nanotube layers for the electrocatalytic hydrogen evolution. We showed that the highest current density of −200 μA/cm^2 collected at −0.4 V vs Ag/AgCl is obtained for the TiO_2 nanotube layer sulfurized at 350 °C, while the blank counterpart generates only −100 μA/cm^2. The sulfurization at temperatures higher than 350 °C does not enhance the current density at −0.4 V but the cathodic peak is extended to more positive potentials. Finally, the sulfurized TiO_2 nanotube layers at 450 °C for 3 h exhibit also an anodic oxida-

tion peak resulting in a significant current density of 1.2 mA/cm^2 at 1 V which is in strong contrast with a few μA/cm^2 generated by the blank TiO_2 nanotube layers.

Acknowledgements

European Research Council (project nr. 638857), Ministry of Youth, Education and Sports of the Czech Republic (projects nr. LM2015082, LQ1601 and CZ.02.1.01/0.0/0.0/16_013/0001829) and Czech Science Foundation (GACR) (project nr. 19-17997S) are acknowledged for financial support of this work.

Appendix A. Supplementary data

Supplementary material related to this article can be found, in the online version, at doi:https://doi.org/10.1016/j.apmt.2019.07.018.

References

[1] A. Fujishima, K. Honda, Electrochemical photolysis of water at a semiconductor electrode, Nature 238 (1972) 37–38, http://dx.doi.org/10.1038/238037a0.
[2] X. Chen, S.S. Mao, Titanium dioxide nanomaterials: synthesis, properties, modifications and applications, Chem. Rev. 107 (2007) 2891–2959, http://dx.doi.org/10.1021/cr0500535.
[3] M.R. Hoffmann, S.T. Martin, W. Choi, D.W. Bahnemann, Environmental applications of semiconductor photocatalysis, Chem. Rev. 95 (1995) 69–96, http://dx.doi.org/10.1021/cr00033a004.
[4] A. Mills, S. Le Hunte, An overview of semiconductor photocatalysis, J. Photochem. Photobiol. A 108 (1997) 1–35, http://dx.doi.org/10.1016/S1010-6030(97)00118-4.
[5] H. Sopha, M. Baudys, M. Krbal, R. Zazpe, J. Prikryl, J. Krysa, J.M. Macak, Scaling up anodic TiO2 nanotube layers for gas phase photocatalysis, Electrochem. Commun. 97 (2018) 91–95, http://dx.doi.org/10.1016/j.elecom.2018.10.025.
[6] B. O'Regan, M. Grätzel, A low-cost, high-efficiency solar cell based on dye-sensitized colloidal TiO2 films, Nature 353 (1991) 373–740, http://dx.doi.org/10.1038/353737a0.
[7] X. Gao, J. Li, J. Baker, Y. Hou, D. Guan, J. Chen, C. Yuan, Enhanced photovoltaic performance of perovskite CH3NH3PbI3 solar cells with freestanding TiO2 nanotube array films, Chem. Commun. 50 (2014) 6368–6371, http://dx.doi.org/10.1039/c4cc01864h.
[8] J.M. Macak, H. Tsuchiya, A. Ghicov, K. Yasuda, R. Hahn, S. Bauer, P. Schmuki, TiO2 nanotubes: self-organized electrochemical formation, properties and applications, Curr. Opin. Solid State Mater. Sci. 11 (2007) 3–18, http://dx.doi.org/10.1016/j.cossms.2007.08.004.
[9] X. Wang, Z. Li, J. Shi, Y. Yu, One-dimensional titanium dioxide nanomaterials: nanowires, nanorods, and nanobelts, Chem. Rev. 114 (2014) 9346–9384, http://dx.doi.org/10.1021/cr400633s.
[10] K. Lee, A. Mazare, P. Schmuki, One-dimensional titanium dioxide nanomaterials: nanotubes, Chem. Rev. 114 (2014) 9385–9454, http://dx.doi.org/10.1021/cr500061m.
[11] T. Umebayashi, T. Yamaki, H. Itoh, K. Asai, Analysis of electronic structures of 3d transition metal-doped TiO2 based on band calculations, J. Phys. Chem. Solids 63 (2002) 1909–1920, http://dx.doi.org/10.1016/S0022-3697(02)00177-4.
[12] D. Dvoranova, V. Brezova, M. Mazur, M.A. Malati, Investigations of metal-doped titanium dioxide photocatalysts, Appl. Catal. B Environ. 37 (2002) 91–105, http://dx.doi.org/10.1016/S0926-3373(01)00335-6.
[13] K. Awazu, M. Fujimaki, C. Rockstuhl, J. Tominaga, H. Murakami, Y. Ohki, N. Yoshida, T. Watanabe, A plasmonic photocatalyst consisting of silver nanoparticles embedded in titanium dioxide, J. Am. Chem. Soc. 130 (2008) 1676–1680, http://dx.doi.org/10.1021/ja076503n.
[14] Q. Wang, R. Jin, M. Zhang, S. Gao, Solvothermal preparation of Fe-doped TiO2 nanotube arrays for enhancement in visible light induced photoelectrochemical performance, J. Alloys Compd. 690 (2017) 139–144, http://dx.doi.org/10.1016/j.jallcom.2016.07.281.
[15] C. Burda, Y. Lou, X. Chen, A.C.S. Samia, J. Stout, J.L. Gole, Enhanced nitrogen doping in TiO2 nanoparticles, Nano Lett. 3 (2003) 1049–1051, http://dx.doi.org/10.1021/nl034332o.
[16] H. Irie, Y. Watanabe, K. Hashimoto, Carbon-doped Anatase TiO2 powders as a visible-light sensitive photocatalyst, Chem. Lett. 32 (2003) 772–773, http://dx.doi.org/10.1246/cl.2003.772.
[17] D. Li, H. Haneda, N.K. Labhsetwar, S. Hishita, N. Ohashi, Visible-light-driven photocatalysis on fluorine-doped TiO2 powders by the creation of surface oxygen vacancies, Chem. Phys. Lett. 401 (2005) 579–584, http://dx.doi.org/10.1016/j.cplett.2004.11.126.
[18] K. Yang, Y. Dai, B. Huang, M.-H. Whangbo, Density functional characterization of the band edges, the band gap states, and the preferred doping sites of halogen-doped TiO2, Chem. Mat. 20 (2008) 6528–6534, http://dx.doi.org/10.1021/cm801741m.
[19] Y.-H. Lin, H.-T. Hsueh, C.-W. Chang, H. Chu, The visible light-driven photodegradation of dimethyl sulfide on S-doped TiO2: characterization, kinetics, and reaction pathways, Appl. Catal. B Environ. 199 (2016) 1–10, http://dx.doi.org/10.1016/j.apcatb.2016.06.024.
[20] R. Asahi, T. Morikawa, T. Ohwaki, K. Aoki, Y. Taga, Visible-light photocatalysis in nitrogen-doped titanium oxides, Science (80-.) 293 (2001) 269–271, http://dx.doi.org/10.1126/SCIENCE.1061051.
[21] A. Ghicov, H. Tsuchiya, R. Hahn, J.M. Macak, A.G. Muñoz, P. Schmuki, TiO2 nanotubes: H+ insertion and strong electrochromic effects, Electrochem. Commun. 8 (2006) 528–532, http://dx.doi.org/10.1016/j.elecom.2006.01.015.
[22] J. Song, M. Zheng, X. Yuan, Q. Li, F. Wang, L. Ma, Y. You, S. Liu, P. Liu, D. Jiang, L. Ma, W. Shen, Electrochemically induced Ti3+self-doping of TiO2 nanotube arrays for improved photoelectrochemicalwater splitting, J. Mater. Sci. 52 (2017) 6976–6986, http://dx.doi.org/10.1007/s10853-017-0930-z.
[23] X. Chen, L. Liu, P.Y. Yu, S.S. Mao, Increasing solar absorption for photocatalysis with black hydrogenated titanium dioxide nanocrystals, Science (80-.) 331 (2011) 746–750, http://dx.doi.org/10.1126/science.1200448.
[24] N. Liu, C. Schneider, D. Freitag, E.M. Zolnhofer, K. Meyer, P. Schmuki, Noble-metal-free photocatalytic H2 generation: active and inactive "Black" TiO2 nanotubes and synergistic effects, Chem. Eur. J. 22 (2016) 13810–13814, http://dx.doi.org/10.1002/chem.201602714.
[25] Q. Wang, J. Qiao, R. Jin, X. Xu, S. Gao, Fabrication of plasmonic AgBr/Ag nanoparticles-sensitized TiO2 nanotube arrays and their enhanced photo-conversion and photoelectrocatalytic properties, J. Power Sources 277 (2015) 480–485, http://dx.doi.org/10.1016/j.jpowsour.2014.08.061.
[26] F. Dvorak, R. Zazpe, M. Krbal, H. Sopha, J. Prikryl, S. Ng, L. Hromadko, F. Bures, J.M. Macak, One-dimensional anodic TiO2 nanotubes coated by atomic layer deposition: towards advanced applications, Appl. Mater. Today 14 (2019) 1–20, http://dx.doi.org/10.1016/j.apmt.2018.11.005.
[27] T. Umebayashi, T. Yamaki, S. Yamamoto, A. Miyashita, S. Tanaka, T. Sumita, K. Asai, Sulfur-doping of rutile-titanium dioxide by ion implantation: Photocurrentspectroscopy and first-principles band calculation studies, J. Appl. Phys. 93 (2003) 5156–5160, http://dx.doi.org/10.1063/1.1565693.
[28] M. Hamadanian, A. Reisi-Vanani, A. Majedi, Preparation and characterization of S-doped TiO2 nanoparticles, effect of calcination temperature and evaluation of photocatalytic activity, Mater. Chem. Phys. 116 (2009) 376–382, http://dx.doi.org/10.1016/j.matchemphys.2009.03.039.
[29] X. Tang, D. Li, Sulfur-doped highly ordered TiO2 nanotubular arrays with visible light response, J. Phys. Chem. C 112 (2008) 5405–5409, http://dx.doi.org/10.1021/jp710468a.
[30] J.W. Zheng, A. Bhattcahrayya, P. Wu, Z. Chen, J. Highfield, Z. Dong, R. Xu, The origin of visible light absorption in chalcogen element (S, Se, and Te)-doped anatase TiO2 photocatalysts, J. Phys. Chem. C 114 (2010) 7063–7069, http://dx.doi.org/10.1021/jp9115035.
[31] T. Umebayashi, T. Yamaki, S. Tanaka, K. Asai, Visible light-induced degradation of methylene blue on S-doped TiO2, Chem. Lett. 32 (2003) 330, http://dx.doi.org/10.1246/cl.2003.330.
[32] C. Han, M. Pelaez, V. Likodimos, A.G. Kontos, P. Falaras, K. O'Shea, D.D. Dionysiou, Innovative visible light-activated sulfur doped TiO2 films for water treatment, Appl. Catal. B Environ. 107 (2011) 77–87, http://dx.doi.org/10.1016/j.apcatb.2011.06.039.
[33] J.C. Yu, W. Ho, J. Yu, H. Yip, P.K. Wong, J. Zhao, Efficient visible-light-induced photocatalytic disinfection on sulfur-doped nanocrystalline titania, Environ. Sci. Technol. 39 (2005) 1175–1179, http://dx.doi.org/10.1021/es035374h.
[34] S. Cravanzola, F. Cesano, F. Gaziano, D. Scarano, Sulfur-doped TiO2: structure and surface properties, Catalysts 7 (2017) 214, http://dx.doi.org/10.3390/catal7070214.
[35] L. Ji, X. Zhou, P. Schmuki, Sulfur and Ti3+ co-doping of TiO2 nanotubes enhance photocatalytic H2 evolution without the use of any co-catalyst, Chem. Asian J. (2019), http://dx.doi.org/10.1002/asia.201900532.
[36] M. Lickleder, G. Cha, R. Hahn, P. Schmuki, Ordered nanotubular titanium disulfide (TiS2) structures: synthesis and use as counter electrodes in dye sensitized solar cells (DSSCs), J. Electrochem. Soc. 166 (2019) H3009–H3013, http://dx.doi.org/10.1149/2.0031905jes.
[37] N.A. Kyerematen, N. Plylahan, A.C.S. Dos Santos, L.V. Taveira, L.F.P. Dick, T. Djenizian, Sulfidated TiO2 nanotubes: a potential 3D cathode material for Li-ion micro batterie, Chem. Commun. 49 (2013) 4205–4207, http://dx.doi.org/10.1039/c2cc36857a.
[38] G.D. Salian, M. Krbal, H. Sopha, C. Lebouin, M.-V. Coulet, J. Michalicka, L. Hromadko, A.T. Tesfaye, J.M. Macak, T. Djenizian, Self-supported sulphurized TiO2 nanotube layers as positive electrode for lithium-ion microbatteries, Appl. Mater. Today 16 (2019) 257–264, http://dx.doi.org/10.1016/j.apmt.2019.05.015.
[39] M. Zhu, C. Zhai, L. Qiu, C. Lu, A.S. Paton, Y. Du, G.M. Cynthia, New method to synthesize S-doped TiO2 with stable and highly efficient photocatalytic performance under indoor sunlight irradiation, ACS sustain, Chem. Eng. 3 (2015) 3123–3129, http://dx.doi.org/10.1021/acssuschemeng.5b01137.
[40] S. Furuseth, Structural properties of the Ti1-xNbxS2 phase, J. Alloy Compd. 178 (1992) 211–215, http://dx.doi.org/10.1016/0925-8388(92)90263-9.
[41] O. Gorochov, A. Katty, N. Le Nagard, C. Levy-Clement, D.M. Schleich, Photoelectrochemical study of TiS3 in aqueous solution, Mater. Res. Bull. 18 (1983) 111–118, http://dx.doi.org/10.1016/0025-5408(83)90178-2.
[42] C.G. Hawkins, A. Whittaker-Brooks, Controlling sulfur vacancies in TiS2–x cathode insertion hosts via the conversion of TiS3 nanobelts for

energy-storage applications, ACS Appl. Nano Mater. 1 (2018) 851–859, http://dx.doi.org/10.1021/acsanm.7b00266.
[43] R.S.C. Smart, W.M. Skinner, A.R. Gerson, XPS of sulphide mineral surfaces: metal-deficient, polysulphides, defects and elemental sulphur, Surf. Interface Anal. 28 (1999) 101–105, http://dx.doi.org/10.1002/(SICI)1096-9918(199908)28:1<101::AID-SIA627>3.0.CO;2-0.
[44] P.S.N. Liu, H. Mirabolghasemi, K. Lee, S.P. Albu, A. Tighineanu, M. Altomare, Anodic TiO2 nanotubes: double walled vs single walled, Faraday Discuss. 164 (2013) 107–116, http://dx.doi.org/10.1039/c3fd00020f.
[45] M. Motola, H. Sopha, M. Krbal, L. Hromádko, Z. Olmrová Zmrhalová, G. Plesch, J.M. Macak, Comparison of photoelectrochemical performance of anodic single- and double-walled TiO2 nanotube layers, Electrochem. Commun. 97 (2018) 1–5, http://dx.doi.org/10.1016/j.elecom.2018.09.015.
[46] A.V. Kolobov, J. Tominaga, Two-dimensional transition-metal dichalcogenides, Springer Series in Materials Science, 2016.
[47] A. Eftekhari, Molybdenum diselenide (MoSe2) for energy storage, catalysis, and optoelectronics, Appl. Mater. Today 8 (2017) 1–17, http://dx.doi.org/10.1016/j.apmt.2017.01.006.
[48] Y. Yu, S.-Y. Huang, Y. Li, S.N. Steinmann, W. Yang, L. Cao, Dependent electrocatalysis of MoS2 for hydrogen evolution, Nano Lett. 14 (2014) 53–58, http://dx.doi.org/10.1021/nl403620g.
[49] K.C. Kwon, S. Choi, K.S. Hong, C.W. Moon, Y.-S. Shim, D.H. Kim, T. Kim, W. Sohn, J.-M. Jeon, C.-H. Lee, Wafer-scale transferable molybdenum disulfide thin-film catalysts for photoelectrochemical hydrogen production, Energy Environ. Sci. 9 (2016) 2240, http://dx.doi.org/10.1039/C6EE00144K.
[50] J. Benson, M. Li, S. Wang, P. Wang, P. Papakonstantinou, Electrocatalytic hydrogen evolution reaction on edges of a few layer molybdenum disulfide nanodots, ACS Appl. Mater. Interfaces 7 (2015) 14113–14122, http://dx.doi.org/10.1021/acsami.5b03399.
[51] Y. Liu, C. Liang, J. Wu, T. Sharifi, H. Xu, Y. Nakanishi, Y. Yang, C.F. Woellne, A. Aliyan, A.A. Martí, B. Xie, R. Vajtai, W. Yang, P.M. Ajayan, Atomic layered titanium sulfide quantum dots as electrocatalysts for enhanced hydrogen evolution reaction, Adv. Mater. Interfaces 5 (2018), 1700895, http://dx.doi.org/10.1002/admi.201700895.
[52] Z. Liu, X. Zhang, B. Wang, M. Xia, S. Gao, X. Liu, A. Zavabeti, J.Z. Ou, K. Kalantar-Zadeh, Y. Wang, Amorphous MoSx-coated TiO2 nanotube arrays for enhanced electrocatalytic hydrogen evolution reaction, J. Phys. Chem. C 122 (2018) 12589–12597, http://dx.doi.org/10.1021/acs.jpcc.8b01678.
[53] X. Liu, S. Gao, P. Yang, B. Wang, J.Z. Ou, Z. Liu, Y. Wang, Synergetic coupling of Pd nanoparticles and amorphous MoSxtoward highlyefficient electrocatalytic hydrogen evolution reactions, Appl. Mater. Today 13 (2018) 158–165, http://dx.doi.org/10.1016/j.apmt.2018.09.001.
[54] Z. Zeng, C. Tan, X. Huang, S. Bao, H. Zhang, Growth of noble metal nanoparticles on single-layer TiS2 and TaS2 nanosheets for hydrogenevolution reaction, Energy Environ. Sci. 7 (2014) 797, http://dx.doi.org/10.1039/c3ee42620c.
[55] Y. Li, H. Wang, L. Xie, Y. Liang, G. Hong, H. Dai, MoS2 nanoparticles grown on graphene: an advanced catalyst for the hydrogen evolution reaction, J. Am. Chem. Soc. 133 (2011) 7296–7299, http://dx.doi.org/10.1021/ja201269b.
[56] J. Kibsgaard, T.F. Jaramillo, Molybdenum phosphosulfide: an active, acid-stable, earth- abundant catalyst for the hydrogen evolution reaction, Angew. Chem. Int. Ed. 53 (2014) 14433–14437, http://dx.doi.org/10.1002/anie.201408222.